

# An asynchronous and parallel time-marching method: Application to three-dimensional MHD simulation of solar wind

SHEN Fang<sup>†</sup>, FENG XueShang & SONG WenBin

SIGMA Weather Group, State Key Laboratory for Space Weather, Center for Space Science and Applied Research, Chinese Academy of Sciences, Beijing 100190, China

**An asynchronous and parallel time-marching method for three-dimensional (3D) time-dependent magnetohydrodynamic (MHD) simulation is used for large-scale solar wind simulation. It uses different local time steps in the corona and the heliosphere according to the local Courant-Friedrichs-Levy (CFL) conditions. The solar wind background with observed solar photospheric magnetic field as input is first presented. The simulation time for the background solar wind by using the asynchronous method is <1/6 of that by using the normal synchronous time-marching method with the same computation precision. Then, we choose the coronal mass ejection (CME) event of 13 November, 2003 as a test case. The time-dependent variations of the pressure and the velocity configured from a CME model at the inner boundary are applied to generate transient structures in order to study the dynamical interaction of a CME with the background solar wind flow between 1 and 230 Rs. This time-marching method is very effective in terms of computation time for large-scale 3D time-dependent numerical MHD problem. In this validation study, we find that this 3D MHD model, with the asynchronous and parallel time-marching method, provides a relatively satisfactory comparison with the ACE spacecraft observations at L1 point.**

asynchronous, parallel, MHD simulation, CME

## 1 Introduction

CMEs and their interplanetary consequences (ICMEs) represent different aspects of the same phenomenon responsible for large geomagnetic storms<sup>[1]</sup>. Because of the great complexity, each aspect has typically been investigated separately, which is useful for revealing the basic underlying physics. In order to obtain a complete picture, one needs to conduct a 3D magnetohydrodynamic (MHD) modeling to consider the coupling between the corona and the interplanetary processes.

For the past ten years, a large amount of work has been done in numerical studies of CMEs and their interplanetary manifestations. Here, we have no intention to review the progress in 3D solar wind simulation, but the following description is only limited to those closely

related to our present topic. In simulating the large scale solar wind, regional combination method and the inner heliospheric model (in super sonic/superAlfvenic region) are usually used in order to achieve a fast convergence. Successful merging of two- and three-dimensional (2D and 3D) MHD coronal and heliospheric models was achieved and reviewed<sup>[2-4]</sup>. Usmanov et al.<sup>[5]</sup> used a global axisymmetric MHD solar wind model with WKB Alfvén waves by combining a time relaxation numerical technique in the 2D solar corona region (1–22 Rs) with

Received July 23, 2008; accepted April 28, 2009

doi: 10.1007/s11431-009-0291-1

<sup>†</sup>Corresponding author (email: fshen@spaceweather.ac.cn)

Supported by the National Natural Science Foundation of China (Grant No. 40874077, 40621003, 40874091, 40536029, 40523006 and 40604019), the National Basic Research Program of China ("973" Project) (Grant No. 2006CB806304), and the Specialized Research Fund for State Key Laboratories

a marching-along-radius method in the outer region (22 Rs–10 AU). The large-scale structure of the solar wind was also simulated by Feng<sup>[6]</sup> and Shen et al.<sup>[7]</sup> by using the 3D MHD regional combination numerical model (hereafter called corona-interplanetary TVD MHD model—COIN-TVD model for brief). The 3D MHD equations were solved by combining a time relaxation numerical technique in the corona with a marching-along-radius method in the heliosphere.

To improve the precision in the heliosphere and save computational cost, we made a modification to the 3D COIN-TVD model mentioned above to realize the whole time-dependent simulation from the solar surface to 1 AU by applying an asynchronous and parallel time-marching method during the simulation. Since all traditional synchronous time-driven methods face the common problems, such as excessive computation and CFL constraint<sup>[8]</sup>, recently a new approach presented by Omelchenko and Karimabadi<sup>[9]</sup> first introduced an asynchronous scheme for drift-diffusion transport. The performance of the new technique was demonstrated in a series of one-dimensional multi-scale plasma modeling<sup>[10]</sup> and gas dynamics test problems<sup>[11]</sup>. Then, a modified asynchronous scheme with local time was proposed by associating independent time tags directly to the interface fluxed between cells and to the source terms within cells in one-dimensional (1D) form, and the performance of this scheme was demonstrated in the 1D application to gas discharges<sup>[12]</sup>. Here, we combine the asynchronous spirit with parallel computation to deal with the large-scale 3D MHD simulation.

In what follows, the asynchronous and parallel time-marching method is first described and then used to simulate the solar wind background and the interplanetary propagation for the November 13, 2003 CME event. Finally, the conclusions are made.

## 2 3D MHD simulation of the solar wind background for CR 2009

In this section, the 3D MHD simulation of the solar wind background for Carrington rotation (CR) 2009 is presented in order to show the asynchronous and parallel time-marching method. The computational domain for this 3D MHD simulation was a Sun-centered spherical coordinate system ( $r, \theta, \varphi$ ) with the  $r$ -axis in the ecliptic plane. The Earth was located at  $r=215$  Rs,  $\theta=0^\circ$ , and

$\varphi=180^\circ$ . The domain covered  $1 \text{ Rs} \leq r \leq 230 \text{ Rs}$ ;  $-75^\circ \leq \theta \leq 75^\circ$ ,  $0^\circ \leq \varphi \leq 360^\circ$ . The grid network was chosen to be  $184(r) \times 75(\theta) \times 180(\varphi)$ . The grid size was uniform in azimuth, with  $\Delta\varphi=2^\circ$ . The radial grid ( $r_i$ ) and the meridional grid ( $\theta_j$ ) were not uniform. In order to obtain a precise computational resolution, we chose for the radial grid:  $r(1) = 1 \text{ Rs}$ ,  $\Delta r(1) = s \times r(1)$ ,  $\Delta r(i) = s \times r(i-1)$ ,  $r(i) = r(i-1) + \Delta r(i-1)$ , where  $s = \pi/90$  between 1 and 22 Rs, and  $s = \pi/120$  between 22 and 230 Rs. For the meridional grid we chose  $\Delta\theta(0^\circ)=1^\circ$ ,  $\Delta\theta(-75^\circ) = \Delta\theta(75^\circ)=3^\circ$ , with a constant increase in  $\Delta\theta$  from  $\theta=0^\circ$  to  $\theta=\pm 75^\circ$ .

The numerical 3D MHD scheme used was a modified total variation diminishing/Lax-Friedrichs (TVD/LF) type scheme<sup>[6,7,13]</sup> with electric field modification method<sup>[14]</sup>. This numerical model satisfied  $\nabla \cdot \mathbf{B} = 0$  to round-off error. This was achieved by the field-interpolated central difference approach for solving the magnetic field<sup>[14]</sup>. The time-dependent 3D ideal MHD equations also included solar rotation and volumetric heating. The equations could be written in a spherical component form at the inertial (non-rotating) reference frame, which was described in detail in our another paper<sup>[7]</sup>.

The applied initial conditions of density ( $\rho$ ), velocity ( $v$ ), and temperature ( $T$ ) were given by the hydrodynamic solar wind solution of Parker<sup>[15]</sup>. The initial magnetic field could be derived from the observed photospheric magnetic field as described by Hu et al.<sup>[16]</sup> Line-of-sight (los) photospheric field ( $B_{\text{los}}$ ) measurements of the Sun were made at Wilcox Solar Observatory (WSO), and are currently available on the web site <http://wso.stanford.edu>. Due to the line saturation effects, the observed magnetic field strength should be modified by a correction factor. Based on the calibration analysis of WSO and other solar observatories<sup>[17,18]</sup>, a saturation factor of 1.8 was chosen for observed data at WSO.

With the assumption that the magnetic field was truly radial in the region of the photosphere where the measurements were taken, the radial magnetic field  $B_r$  was specified at the inner boundary  $r=1$  Rs by the relationship  $B_r = B_{\text{los}}/\cos \theta$ , where  $\theta$  was the colatitude measured from the solar north pole<sup>[19,20]</sup>. By using the giving  $B_r$  distribution at inner boundary and the multipolar expansion model, the distribution of magnetic field could be deduced from 1 to 230 Rs. At the solar base, we fixed the plasma parameters to be the same as the initial data. At the outer boundary of 230 Rs and the two latitudinal

boundaries, linear extrapolations were used to specify the parameters.

During our simulation, the time step ( $\Delta t$ ) was restricted by the CFL condition<sup>[13]</sup>. For the system to remain numerically stable, generally the time integration step of the system is limited by the minimum of the CFL condition all over the domain. Thus, the time-dependent 3D large-scale MHD model requires a lot of computing resources and needs so much time to arrive at the steady state. To save computation time, and maintain simulation accuracy, we introduced an asynchronous and parallel time-marching method by using different local time steps (adapted to the local CFL condition) in the corona (1 to 22 Rs) and the heliosphere (22 to 230 Rs), and applying parallel computation in  $r$ -direction.

Figure 1 shows the relationship between the local time steps of the corona ( $\Delta t_c$ ) and the heliosphere ( $\Delta t_h$ ). These local time steps were computed separately according to the local CFL condition equations in their associated regions. To make the local time steps of the corona and the heliosphere consistent with each other, we assumed the following conditions:

$$\text{If } \sum_{i=1}^{n-1} (\Delta t_c)_i < \sum_{j=1}^m (\Delta t_h)_j \text{ and } \sum_{i=1}^n (\Delta t_c)_i > \sum_{j=1}^m (\Delta t_h)_j \quad (n \neq$$

$m$ ), then if  $m=1$ , we set  $(\Delta t_h)'_1 = \sum_{i=1}^n (\Delta t_c)_i$ ; and if  $m \neq 1$ ,

we set  $(\Delta t_h)'_m = \sum_{i=1}^n (\Delta t_c)_i - \sum_{j=1}^{m-1} (\Delta t_h)_j$ . Then,  $(\Delta t_h)'$  was

used as the corrected local time step in the heliosphere. In this way, using 30 parallel programming

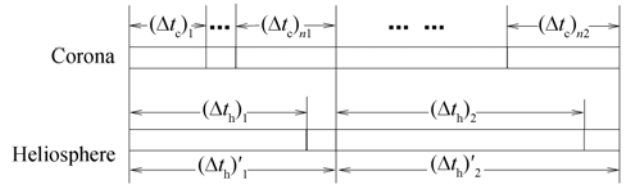


**Figure 1** The relationship between the local time steps of the corona ( $\Delta t_c$ ) and the heliosphere ( $\Delta t_h$ ).

processes on a 20-node PC cluster with two 3.0 GHz Intel Xeon CPUs per node interconnected with Gigabit Ethernet, we only needed less than 50 h of CPU time to reach the steady state, corresponding to the physical time of 100 h. We also made a test of using the normal time steps limited by the minimum of the CFL condition all over the domain (1–230 Rs) to solve the same 3D MHD equations, and it took >300 h to get the steady-state (physical time=100 h). These two simulations used the same mesh, computation domain, MHD scheme, and the number of parallel programming nodes, and the simulation results were almost the same, while the simulation time of the normal method was 5 times more than that of the asynchronous and parallel time-marching method. Some simulation results of the asynchronous method and the traditional synchronous method are discussed below.

Figure 2 shows the calculated steady-state magnetic field topology in the meridional plane at  $\varphi=180^\circ$  (Figure 2(a)) and equatorial plane (Figure 2(b)) at 100 h. The well-known Archimedes' spiral lines appear in Figure 2(b). Figure 3 shows the ambient state at 100 h after the time-dependent solution is obtained based on the asynchronous time-marching method (black lines) and traditional synchronous time-marching method (red

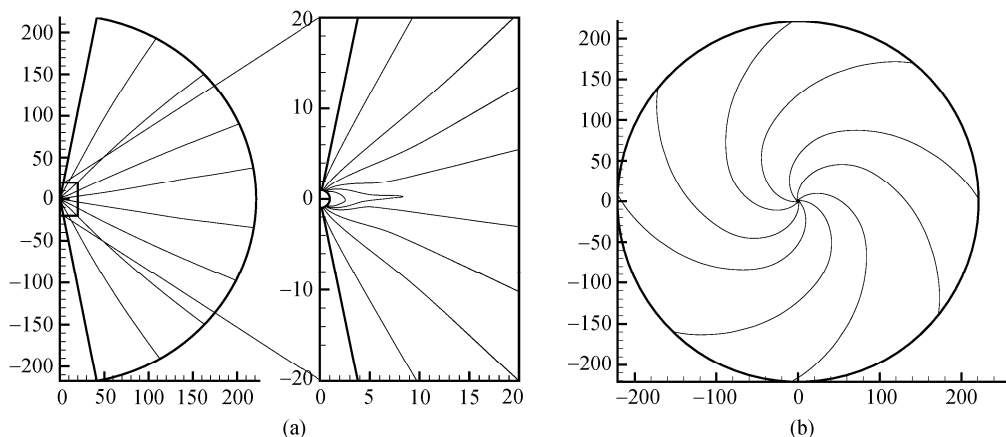


**Figure 2** The calculated steady-state solution for magnetic field in the meridional plane at  $\varphi=180^\circ$  from 1 to 230 Rs and at smaller scale (a), and equatorial plane from 1 to 230 Rs at 100 h (b). The units of the  $x$ - $y$  axis are Rs.

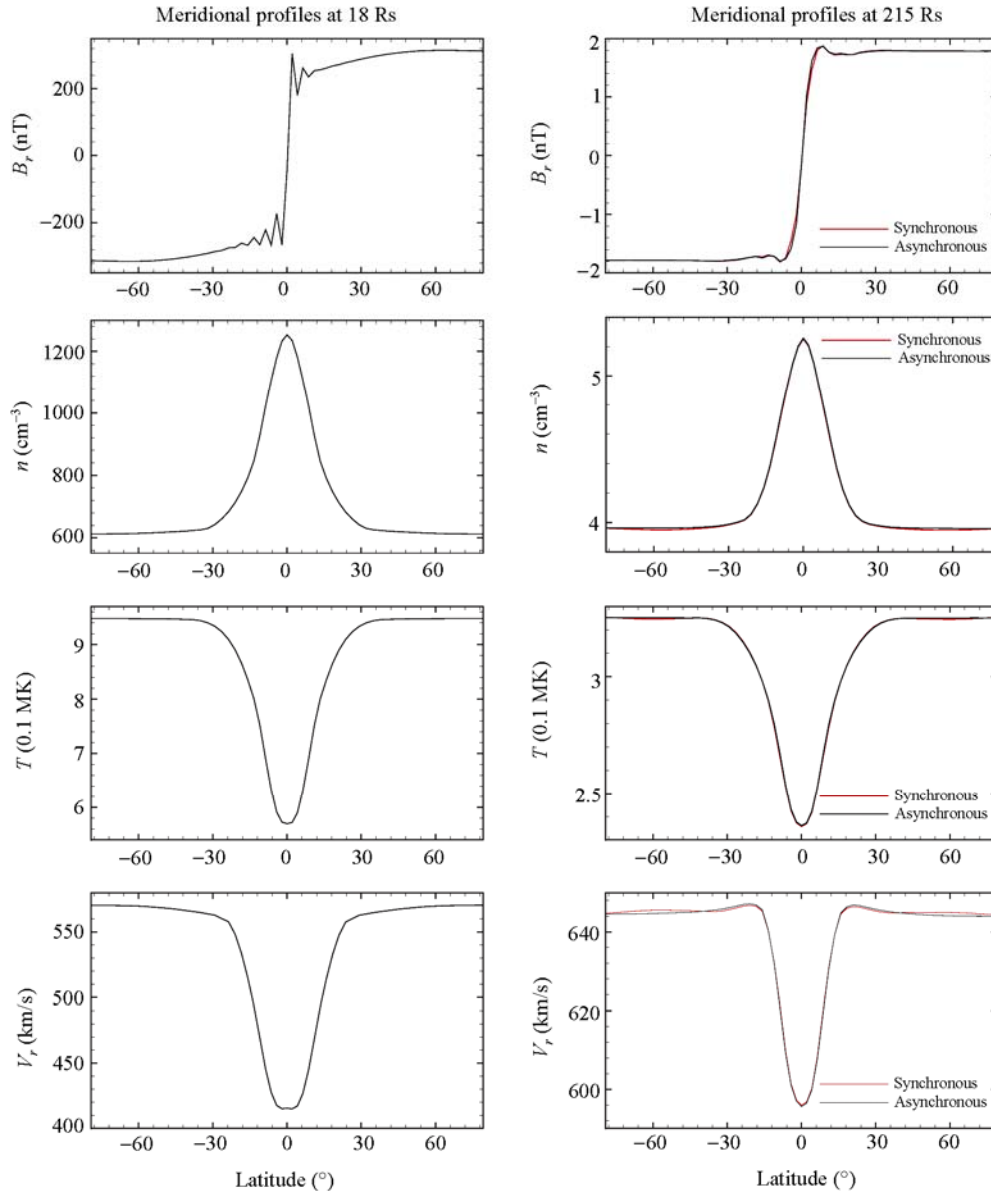


**Figure 3** Profiles of the radial magnetic field, proton number density, temperature, and the radial velocity at  $r=18$  Rs (corona) and  $r=215$  Rs (heliosphere) (meridional profiles at  $\varphi=180^\circ$ ) are shown in the left and right panels, respectively. The red lines and black lines at  $r=215$  Rs separately represent the traditional synchronous and the asynchronous simulation results. At  $r=18$  Rs, the results of the synchronous and the asynchronous simulation are entirely superposed, so we only use black lines.

lines). The agreement between the two simulations is excellent and is within noise levels. Profiles of the radial magnetic field, proton number density, temperature, and the radial velocity at  $r=18$  Rs (corona) and  $r=215$  Rs (heliosphere) (meridional profiles at  $\varphi=180^\circ$ ) are shown in the left and right panels, respectively. Both the configurations of the corona and the heliosphere consist of a dense and slow flow near the current sheet. The range of latitude is about  $\pm 25^\circ$ . The absolute value of the radial magnetic field almost remains constant, independent

with latitude, which is consistent with the Ulysses observation<sup>[21–23]</sup>.

### 3 Numerical simulation of November 13, 2003 CME event

This part is devoted to the numerical simulation of November 13, 2003 CME event in order to show the applicability of the asynchronous and parallel time-marching method in interplanetary transient study. The November

13, 2003 has been studied with the 3D pure hydrodynamic numerical simulation by Ogawa et al.<sup>[24]</sup>. From SOHO/LASCO CME catalog, the CME was first observed by the C2 coronagraph on 13 November 2003 at 09:30 UT, and the observed velocity of the CME was 1141 km/s. An associated X-ray flare occurred at N01E90. The CME arrived at L1 point ( $1.5 \times 10^9$  m from the Earth to sunward) on 16 November 2003 at 05:40 UT based on the ACE spacecraft observation, which showed that the interplanetary disturbance caused by this CME took about 68 h to reach the L1 point.

With the steady-state solar wind produced in the last section, we input a CME model into the inner boundary by modeling a CME as follows:

$$\begin{cases} V_{\text{CME}}(t, \xi) = V_{\text{max}} A(\xi) C(t), \\ \rho_{\text{CME}}(t, \xi) = \rho_{\text{max}} A(\xi) C(t), \\ T_{\text{CME}}(t, \xi) = T_{\text{max}} A(\xi) C(t), \end{cases}$$

where

$$A(\xi) = \cos\left(\frac{\pi\xi}{2\xi_0}\right), \quad 0 \leq \xi \leq \xi_0,$$

$$C(t) = \begin{cases} \frac{t}{\tau_1}, & 0 \leq t < \tau_1, \\ 1, & \tau_1 \leq t < \tau_1 + \tau_m, \\ \frac{\tau_1 + \tau_m + \tau_2 - t}{\tau_2}, & \tau_1 + \tau_m \leq t \leq \tau_1 + \tau_m + \tau_2, \end{cases}$$

with  $V_{\text{CME}}$ ,  $\rho_{\text{CME}}$  and  $T_{\text{CME}}$  being the radial velocity, density and temperature of the input CME, respectively.  $V_{\text{max}}$ ,  $\rho_{\text{max}}$  and  $T_{\text{max}}$  represent the amplitude of the perturbation of the radial velocity, density, and temperature, respectively.  $\xi$ ,  $\xi_0$ ,  $\tau_1$ ,  $\tau_2$  and  $\tau_m$  are the angle to the axis of CME cone, angular radius of CME, ramp-up time, ramp-down time, and duration time of the perturbation at maximum value, respectively<sup>[7,24]</sup>.

This perturbation will be started by the following relation:

$$\begin{cases} v_r = v_{r0} + v_{\text{CME}}(t, \xi), \\ \rho = \rho_0 + \rho_{\text{CME}}(t, \xi), \\ T = T_0 + T_{\text{CME}}(t, \xi), \end{cases}$$

where  $v_{r0}$ ,  $\rho_0$  and  $T_0$  are the background values of the radial velocity, density, and temperature calculated in Section 2. In our simulation, we set  $V_{\text{max}}=1141$  km/s,  $\xi_0=15^\circ$  and  $\tau_1=\tau_2=1$  h. The CME was assumed to occur on the equator plane, longitude= $E25^\circ$  and  $\tau_m=4$  h, which were also used by Ogawa et al.<sup>[24]</sup> to fit the observation

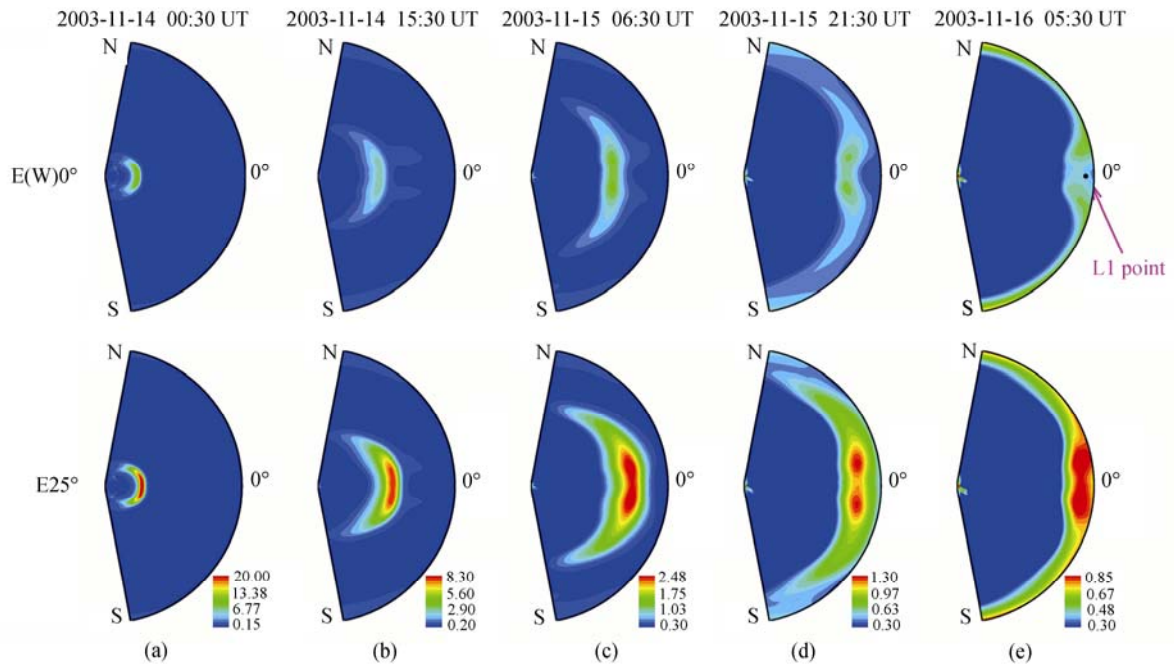
by ACE spacecraft at L1 point.

The relative density  $((\rho - \rho_0)/\rho_0)$ , where  $\rho$  is the total density, and  $\rho_0$  is the density of the background wind, is shown in Figures 4 and 5 at five consecutive times (Figures 5 and 6). Figure 4 shows the profiles for the relative density at a constant meridional angle of  $\varphi=180^\circ$  (top panel, the Earth location) and  $\varphi=155^\circ$  (bottom panel, the CME's longitude). Figure 5 shows the relative density on the surfaces of three angular cones that are centered at the Sun's center:  $20^\circ$  North (top panel);  $0^\circ$  (middle panel, the Earth location and the CME's heliolatitude); and  $20^\circ$  South (bottom panel). The radial scales both in Figures 5 and 6 were from the solar surface to 230 Rs.

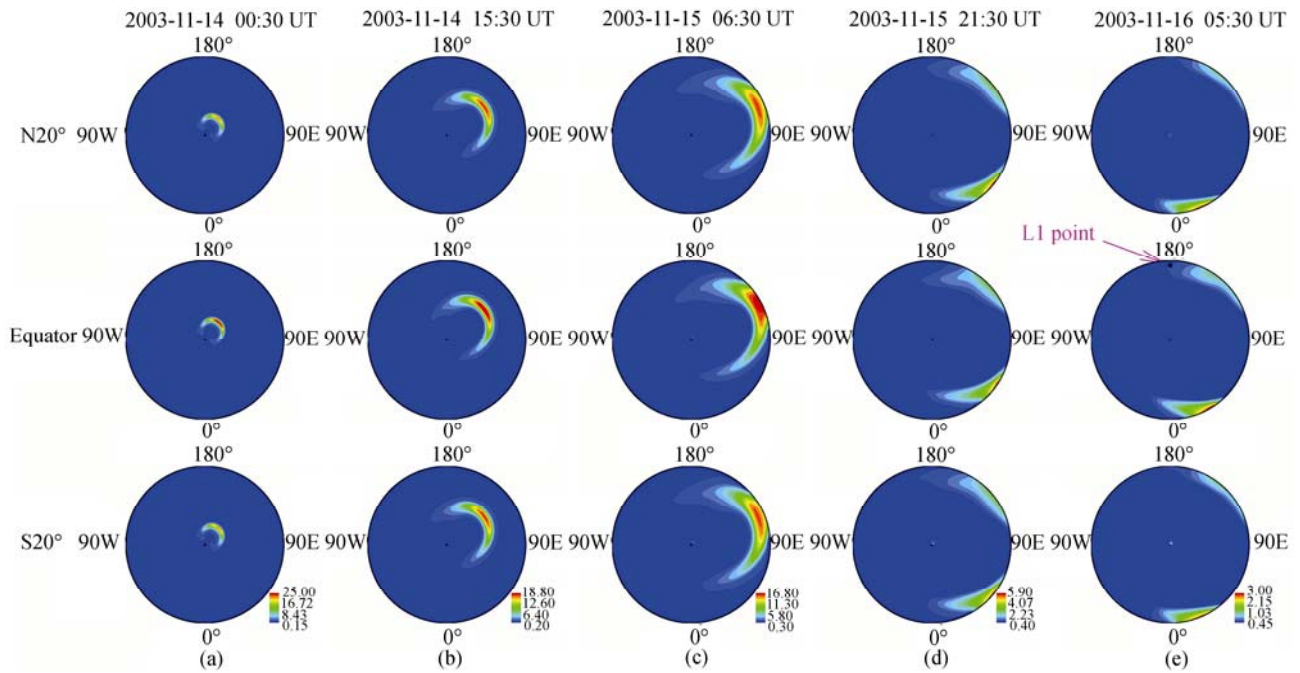
In Figures 4 and 5, the CME is shown to be stronger and faster in the East and in the Equator than in the plane of meridional angle of  $0^\circ$  and in the north or in the south, respectively. This may be due to the fact that the source of CME was located at N(S)0E25.

Figure 6 shows the plots of the total magnetic field strength ( $|B|$ ), the  $x$ ,  $y$ , and  $z$  components ( $B_x$ ,  $B_y$ , and  $B_z$ ) of the magnetic field in the GSE coordinate system, the density ( $\rho$ ), the temperature ( $T$ ) and the magnitude of the bulk velocity ( $v$ ) at L1 point, respectively from the top panel to the bottom panel. Each panel describes the comparison of the computed plasma parameters with the observed parameters. This figure clearly indicates a quantitative resemblance between the simulated and the measured results, such as the maxima of  $|B|$ ,  $B_x$  and  $B_y$ , the maxima of the density and the velocity, the low density and temperature, and the decreasing  $|B|$ , density and temperature.

One of the reasons why quantitative agreement was not obtained in Figure 6 is that the present model, like many others already mentioned, is only a single-fluid model. More importantly, there exist other two extremely important and still unsolved reasons as pointed out by Dryer<sup>[25]</sup> and now recognized by many other modelers<sup>[7,26-28]</sup>. These two reasons are: (1) Uncertainty of the initial realistic solar wind and the IMF background conditions, and (2) uncertainty of the appropriate solar observations to use for "mimicking" solar flare/filament and CME initiation input pulse conditions. In the ambient, pre-CME stage, the simulated radial velocity near the equator was  $\sim 590$  km/s as shown in Figure 3, and in the ICME stage, it's maximal value increased to  $\sim 750$  km/s as seen from Figure 6. In fact, these values



**Figure 4** Evolution of the density contours  $((\rho - \rho_0)/\rho_0)$  of the constant meridional angle of  $\varphi = 180^\circ$  (top panel) and  $\varphi = 155^\circ$  (bottom panel) at five consecutive times (a)–(e).



**Figure 5** Evolution of the density contours  $((\rho - \rho_0)/\rho_0)$  at five consecutive times (a)–(e). The top, middle and bottom panels represent the constant conical angles of  $20^\circ\text{N}$ ,  $0^\circ$  and  $20^\circ\text{S}$ .

were a little higher than the observation. The reason for this might be from our volumetric heating. The heating process is unclear up to now. The choice of such a heating may bring some favorable results but not all. To some extent, using more observational data to constrain the model may avoid the uncertainty of the initial arbi-

trarily-selected solar wind conditions. But, it is still very challenging to mimic the realistic solar flare/filament eruption and CME initiation. It is believed that more solar and interplanetary observations will clarify these uncertainties.

From the top panel of Figure 4(e), the middle panel of

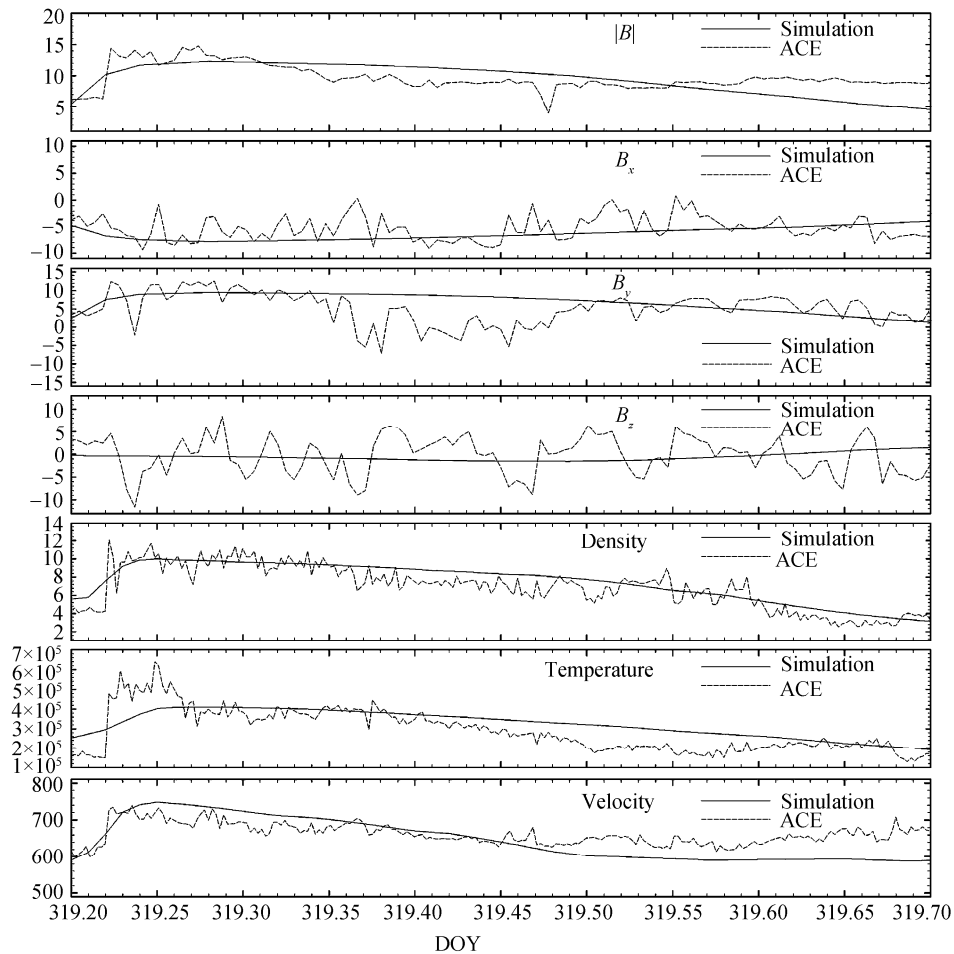


**Figure 6** The comparison of the MHD simulation of magnetic field and plasma parameters with the measured (ACE spacecraft) magnetic field and the solar wind parameters at L1 point in 2003. The solid lines denote simulation parameters, (top to bottom) the magnetic field strength  $|B|$  (nT),  $B_x$  (nT),  $B_y$  (nT),  $B_z$  (nT) at GSE coordinate system, the number density ( $\text{cm}^{-3}$ ), the plasma temperature (K) and the magnitude of the bulk velocity (km/s). The dashed lines denote the measured parameters by ACE, (top to bottom) the magnetic field strength  $|B|$  (nT),  $B_x$  (nT),  $B_y$  (nT),  $B_z$  (nT) at GSE coordinate system, the proton density ( $\text{cm}^{-3}$ ), the proton temperature (K) and the magnitude of the bulk velocity (km/s).

Figure 5(e), and total magnetic field, density, temperature, and velocity profile in Figure 6, we notice that the CME arrival time from the Sun to L1 point was about 68 h, which is consistent with the observation of Section 3. By examining simultaneously the computed density, temperature, and velocity profiles shown in Figure 6, we can see that the largest density enhancement can be identified with the plasma compressed in the helmet dome and the additional plasma swept up by the system in the undisturbed corona during the initial CME propagation. The plasmas in this region were hot, as seen in the temperature profile (Figure 6), because this represents the shocked, compressed plasma. It is noticeable that this asynchronous and parallel time-marching method is equally efficient in this 3D CME modeling as that in the 3D background solar wind, because they use the same simulation model, only the inner boundary

condition is different.

This event has been studied previously with the use of 3D pure hydrodynamic model<sup>[24]</sup>. Ogawa et al.<sup>[24]</sup> applied a 3D AMR hydrodynamic code to simulate the interplanetary shock wave by a CME model as above. They provided the comparison of ACE observation with their numerical results of density and velocity at L1.

We should stress again that our one-fluid (proton) model can not account for the high temperature in a magnetic cloud and the anti-correlation between the electron temperature and density<sup>[29,30]</sup>.

## 4 Conclusions

In conclusion, an asynchronous and parallel time-marching method was presented for the 3D time-dependent solar wind MHD simulation. This method uses

different local time steps in the corona and the heliosphere according to the local CFL condition equations in their own regions. To make the local time steps of the corona and the heliosphere consistent with each other, we employed a coupling-correction method adapted to the local time step of the corona.

Using the asynchronous and parallel time-marching method, we chose the CME event of 13 November 2003 as a test case to carry out the 3D study of the large-scale background solar wind structures, and the propagation of the specific ICME and its shock wave in a nonuniform background solar wind flow derived from observed magnetic field at the solar surface. Our numerical results of the background solar wind are quite consistent with

the observation results. The simulation time of the asynchronous and parallel time-marching method was only 1/6 that of the normal time-marching method, while the computation precision was not influenced. The dynamical interaction of 13 November 2003 CME event with the background solar wind flow between 1 and 230 Rs was also investigated by introducing a time-dependent pulse at the inner boundary to mimic the effects of a filament eruption. This study shows that the 3D MHD model with asynchronous and parallel time-marching method can also provide us a relatively satisfactory comparison between the time-dependent numerical MHD results with those of the ACE spacecraft observations at L1.

- 1 Gosling J T. Coronal mass ejections and magnetic flux ropes in interplanetary space. In: Priest E R, Lee L C, Russell C T, eds. *Physics of Magnetic Flux Ropes*. Geophys Monogr. Washington D. C.: AGU, 1990, 58: 343–364
- 2 Wu S T, Guo W P, Dryer M, et al. Dynamical evolution of a coronal streamer-flux rope system: II. A self-consistent non-planar magneto-hydrodynamic solution. *Sol Phys*, 1997, 170(2): 265–282
- 3 Wu S T, Guo W P, Michels D J, et al. MHD description of the dynamical relationships between a flux rope, streamer, coronal mass ejection, and magnetic cloud: An analysis of the January 1997 Sun-Earth connection event. *J Geophys Res*, 1999, 104(A7): 14789–14802
- 4 Odstrcil D, Linker J A, Lionello R, et al. Merging of coronal and heliospheric numerical 2-D MHD models. *J Geophys Res*, 2002, 107(A12): SSH 14-1, 1493
- 5 Usmanov A V, Goldstein M L, Besser B P, et al. A global MHD solar wind model with WKB Alfvén waves: Comparison with Ulysses data. *J Geophys Res*, 2000, 105(A6): 12675–12696
- 6 Feng X. A comparative study on 3-D solar wind structure observed by Ulysses and MHD simulation. *Chin Sci Bull*, 2005, 50(7): 672–678
- 7 Shen F, Feng X, Wu S T, et al. Three-dimensional MHD simulation of CMEs in three-dimensional background solar wind with the self-consistent structure on the source surface as input: Numerical simulation of the January 1997 Sun-Earth connection event. *J Geophys Res*, 2007, 112(A6): A06109
- 8 Karimabadi H, Driscoll J, Omelchenko Y A, et al. A new asynchronous methodology for modeling of physical systems: breaking the curse of Courant condition. *J Comput Phys*, 2005, 205(2): 755–775
- 9 Omelchenko Y A, Karimabadi H. Self-adaptive time integration of flux-conservative equations with sources. *J Comput Phys*, 2006, 216(1): 179–194
- 10 Omelchenko Y A, Karimabadi H. Event-driven hybrid particle-in-cell simulation: a new paradigm for multi-scale plasma modeling. *J Comput Phys*, 2006, 216(1): 153–178
- 11 Omelchenko Y A, Karimabadi H. A time-accurate explicit multi-scale technique for gas dynamics. *J Comput Phys*, 2007, 226(1): 282–300
- 12 Unfer T, Boeuf J P, Rogier F, et al. An asynchronous scheme with local time stepping for multi-scale transport problems: Application to gas discharges. *J Comput Phys*, 2007, 227(2): 898–918
- 13 Feng X. A class of TVD type combined numerical scheme for MHD equations and its application to MHD numerical simulation (in Chinese). *Chin J Space Sci*, 2002, 22(4): 300–308
- 14 Tóth G. The  $\nabla \cdot B = 0$  constraint in shock-capturing magnetohydrodynamics codes. *J Comput Phys*, 2000, 161(2): 605–652
- 15 Parker E N. *Interplanetary Dynamical Processes*. New York: Wiley-Interscience, 1963
- 16 Hu Y, Feng X, Wu S T, et al. Three-dimensional MHD modeling of the global corona throughout Solar Cycle 23. *J Geophys Res*, 2008, 113(A3): A03106
- 17 Svalgaard L, Duvall T L, Scherrer P H. The strength of the sun's polar fields. *Sol Phys*, 1978, 58(2): 225–239
- 18 Svalgaard L. How good (or bad) are the inner boundary conditions for heliospheric solar wind modeling. SHINE 2006 Workshop. Utah: Rice University, 2006
- 19 Wang Y M, Sheeley Jr N R. On potential field models of the solar corona. *Astrophys J*, 1992, 392(1): 310–319
- 20 Luhmann J G, Li Y, Arge C N, et al. Solar cycle changes in coronal holes and space weather cycles. *J Geophys Res*, 2002, 107(A8): 1154
- 21 McComas D J, Barraclough B L, Funsten H O, et al. Solar wind observations over Ulysses' first full polar orbit. *J Geophys Res*, 2000, 105(A5): 10419–10434
- 22 McComas D J, Elliott H A, Schwadron N A, et al. The three-dimensional solar wind around solar maximum. *Geophys Res Lett*, 2003, 30(10): 24-1
- 23 McComas D J, Elliott H A, Gosling J T, et al. Ulysses observations of very different heliosphere structure during the declining phase of solar activity cycle 23. *Geophys Res Lett*, 2006, 33(9): L09102
- 24 Ogawa T, Den M, Tanaka T. Three-dimensional hydrodynamic code for interplanetary shock wave. In: *Proceedings of ISSS-7*. Kyoto: Kyoto University, 2005. 26–28
- 25 Dryer M. Multi-dimensional MHD simulation of solar-generated disturbances: Space weather forecasting of geomagnetic storms. *AIAA J*, 1998, 36(3): 365–370
- 26 Fry C D, Sun W, Deehr C S, et al. Improvements to the HAF solar wind model for space weather predictions. *J Geophys Res*, 2001, 106(A10): 20985–21002
- 27 Odstrcil D, Riley P, Zhao X P. Numerical simulation of the 12 May 1997 interplanetary CME event. *J Geophys Res*, 2004, 109(A2): A02116
- 28 Zhou Y F, Feng X, Wu S T. Numerical simulation of the 12 May 1997 CME event. *Chin Phys Lett*, 2008, 25(2): 790–793
- 29 Lepping R P, Jones J A, Burlaga L F. Magnetic field structure of interplanetary magnetic clouds at 1AU. *J Geophys Res*, 1990, 95(A8): 957–965
- 30 Lynch B J, Zurbuchen T H, Fisk L A, et al. Internal structure of magnetic clouds: plasma and composition. *J Geophys Res*, 2003, 108(A6): SSH 6-1, 1239